

# *Ab initio* determination of spin Hamiltonians with anisotropic exchange interactions: The case of the pyrochlore ferromagnet $\text{Lu}_2\text{V}_2\text{O}_7$

Kira Riedl,<sup>1,\*</sup> Daniel Guterding,<sup>1</sup> Harald O. Jeschke,<sup>1</sup> Michel J. P. Gingras,<sup>2,3,4</sup> and Roser Valentí<sup>1</sup><sup>1</sup>*Institut für Theoretische Physik, Goethe-Universität Frankfurt, Max-von-Laue-Straße 1, 60438 Frankfurt am Main, Germany*<sup>2</sup>*Department of Physics and Astronomy, University of Waterloo, Ontario, N2L 3G1, Canada*<sup>3</sup>*Perimeter Institute for Theoretical Physics, Waterloo, Ontario, N2L 2Y5, Canada*<sup>4</sup>*Canadian Institute for Advanced Research, 180 Dundas Street West, Suite 1400, Toronto, Ontario, M5G 1Z8, Canada*

(Received 12 April 2016; revised manuscript received 7 June 2016; published 8 July 2016)

We present a general framework for deriving effective spin Hamiltonians of correlated magnetic systems based on a combination of relativistic *ab initio* density functional theory calculations, exact diagonalization of a generalized Hubbard Hamiltonian on finite clusters, and spin projections onto the low-energy subspace. A key motivation is to determine anisotropic bilinear exchange couplings in materials of interest. As an example, we apply this method to the pyrochlore  $\text{Lu}_2\text{V}_2\text{O}_7$  where the vanadium ions form a lattice of corner-sharing spin-1/2 tetrahedra. In this compound, anisotropic Dzyaloshinskii-Moriya interactions (DMIs) play an essential role in inducing a magnon Hall effect. We obtain quantitative estimates of the nearest-neighbor Heisenberg exchange, the DMI, and the symmetric part of the anisotropic exchange tensor. Finally, we compare our results with experimental ones on the  $\text{Lu}_2\text{V}_2\text{O}_7$  compound.

DOI: [10.1103/PhysRevB.94.014410](https://doi.org/10.1103/PhysRevB.94.014410)

## I. INTRODUCTION

The Heisenberg Hamiltonian and its extensions are among the most successful models for describing magnetism in correlated systems [1,2]. However, for an accurate description of real material properties, a sound understanding of the role of the lattice structure (e.g., superexchange pathways) and its consequence on the spin-spin exchange parameters is indispensable. Various methods for determining exchange parameters for real materials exist. A popular one consists of fitting calculated properties obtained by assuming a particular form of the spin Hamiltonian to experimental data (specific heat, magnetic susceptibility, magnetization, inelastic neutron scattering, etc.) [3–6]. A complementary procedure that is gaining popularity is to estimate the coupling constants of the Heisenberg Hamiltonian from methods based on first principles, such as mapping total energies obtained from spin-polarized density functional theory (DFT) calculations to a Heisenberg model [5,7–12]. Both approaches are useful for providing information on Heisenberg-only interactions. These become, however, problematic when terms other than rotationally invariant (isotropic) Heisenberg exchange  $\mathcal{J}_{ij}(\vec{S}_i \cdot \vec{S}_j)$  are not negligible, as it happens in rare-earth pyrochlore compounds [13]. Even when anisotropic terms are small, they can play a crucial role in the physics of the system [14,15]. Common examples of such anisotropic couplings are the off-diagonal Dzyaloshinskii-Moriya vector  $\vec{D}_{ij}$  and the traceless symmetric tensor  $\hat{K}_{ij}$ :

$$H_{\text{spin}} = \mathcal{J}_{ij}(\vec{S}_i \cdot \vec{S}_j) + \vec{D}_{ij} \cdot (\vec{S}_i \times \vec{S}_j) + \vec{S}_i \cdot \hat{K}_{ij} \cdot \vec{S}_j. \quad (1)$$

By broadly aiming to obtain reliable quantitative estimates of the coupling constants in a general spin Hamiltonian such as that of Eq. (1), we explore here, as a first motivation for our work, a method that combines DFT calculations

with exact diagonalization of the electronic (Hubbard-like) Hamiltonian on finite clusters. This approach does not depend on experimental input, except for the crystal structure.

As a specific application of the method, we evaluate the bilinear spin-spin coupling constants in Eq. (1) of the insulating  $\text{Lu}_2\text{V}_2\text{O}_7$  pyrochlore ferromagnet. This material has recently been proposed as a candidate topological magnon insulator with chiral edge states [16,17] and evidence for a magnon Hall effect has also been reported [18]. The magnetic properties of  $\text{Lu}_2\text{V}_2\text{O}_7$  are dominated by corner-sharing spin-1/2 vanadium tetrahedra (see Fig. 1). Due to the lack of bond-inversion symmetry for the pyrochlore lattice [19], the Dzyaloshinskii-Moriya interaction (DMI) of spin-orbit origin [20,21] is allowed by symmetry and may not be negligible. The DMI is expected to play an essential role on the observed magnon Hall effect in  $\text{Lu}_2\text{V}_2\text{O}_7$  and there is a debate about the magnitude of the principal spin-spin interactions in this material. The need to better understand the scale of the anisotropic interactions in contemporary magnetic systems and their role on topological magnon transport is further emphasized by the observation of such phenomena in materials [22,23] other than  $\text{Lu}_2\text{V}_2\text{O}_7$ . From a broader context, the latter material may then possibly be viewed as an important test bench for establishing close contact between theory and experiment.

Coming back to  $\text{Lu}_2\text{V}_2\text{O}_7$ , experimental and theoretical results have been reported for the nearest-neighbor Heisenberg exchange,  $\mathcal{J}_{ij}$ , and the Dzyaloshinskii-Moriya vector,  $\vec{D}_{ij}$ . However, no consensus has yet emerged on the value of these two spin-spin couplings. Fitting transport and magnetic specific heat data on  $\text{Lu}_2\text{V}_2\text{O}_7$  [18] leads to ferromagnetic (negative)  $\mathcal{J}_{ij} \simeq -3.4$  meV [24] and  $|\vec{D}_{ij}|/|\mathcal{J}_{ij}| \simeq 1/3$ . In contrast, recent inelastic neutron scattering measurements [25] indicate that  $|\vec{D}_{ij}|/|\mathcal{J}_{ij}| \simeq 0.18$ . On the other hand, Xiang *et al.* [26] obtained  $|\vec{D}_{ij}|/|\mathcal{J}_{ij}| = 0.048$  by mapping DFT total energies to a spin Hamiltonian. This ratio is one order of magnitude smaller than the values obtained from fitting to experimental data. However, one should note that Ref. [26]

\*riedl@itp.uni-frankfurt.de

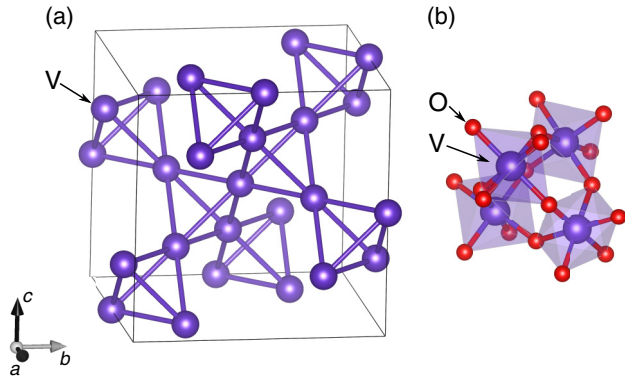


FIG. 1. (a) Network of corner-sharing vanadium tetrahedra in the pyrochlore  $\text{Lu}_2\text{V}_2\text{O}_7$ . (b) Oxygen environment around a vanadium tetrahedron.

includes an additional single-ion anisotropy term in the effective spin Hamiltonian used to parametrize the energy of magnetic moment configurations. In a quantum spin-1/2 Hamiltonian, any such even-power term should, however, be absent as they are trivially proportional to the identity (Pauli  $\sigma_0$ ) matrix. Considering the disparities between the values so far determined for  $\mathcal{J}_{ij}$  and  $\tilde{\mathcal{D}}_{ij}$ , one is naturally led to ask whether additional symmetry-allowed terms, such as the symmetric tensor  $\tilde{\mathcal{K}}_{ij}$  in Eq. (1), are truly negligible in this compound. It is therefore of some importance to determine such couplings consistently within a well-defined calculational procedure; this is the second main motivation for our work.

The paper is organized as follows. Section II discusses the various steps necessary to establish the generalized spin Hamiltonian that we seek. We first present the framework for obtaining tight-binding parameters and the spin-orbit coupling constant  $\lambda$  out of relativistic DFT calculations. In a second step, we perform an exact diagonalization of a generalized Hubbard Hamiltonian that includes the *ab initio* tight-binding parameters and  $\lambda$ . Introducing effective spin-1/2 operators, we project the results on the low-energy subspace of the system to extract an effective spin Hamiltonian allowing us to determine the various exchange coupling constants. The method is applied to  $\text{Lu}_2\text{V}_2\text{O}_7$  where we compare briefly to experimental results. We conclude the paper with a summary in Sec. III.

## II. GENERALIZED MODEL HAMILTONIAN

### A. *Ab initio* determination of the tight-binding hopping and spin-orbit parameters

Our starting Hamiltonian is a generalized multiorbital Hubbard model for  $d$  electrons that includes spin-orbit coupling (SOC):

$$H_{\text{tot}} = H_{\text{hop}} + H_{\text{soc}} + H_{\text{int}}, \quad (2)$$

where

$$H_{\text{hop}} = \sum_{ij} \sum_{\alpha\beta} t_{i\alpha,j\beta} d_{i\alpha}^\dagger d_{j\beta} \quad (3)$$

is the hopping term with hopping parameters  $t_{i\alpha,j\beta}$  where  $i, j$  are site indices and  $\alpha, \beta$  are orbital indices [27].

$$H_{\text{soc}} = \lambda \sum_i \sum_{\alpha\beta} \sum_{\sigma\sigma'} \langle i\alpha\sigma | \vec{L} \cdot \vec{S} | i\beta\sigma' \rangle d_{i\alpha\sigma}^\dagger d_{i\beta\sigma'}, \quad (4)$$

is the spin-orbit term where  $\lambda$  is the strength of the on-site spin-orbit coupling and  $\sigma$  and  $\sigma'$  are the spin component indices.

$$\begin{aligned} H_{\text{int}} = & \sum_i \sum_{\alpha\beta} U_{\alpha\beta} n_{i\alpha\uparrow} n_{i\beta\downarrow} \\ & + \frac{1}{2} \sum_{i\sigma} \sum_{\alpha\neq\beta} (U_{\alpha\beta} - J_{\alpha\beta}) n_{i\alpha\sigma} n_{i\beta\sigma} \\ & + \sum_i \sum_{\alpha\neq\beta} J_{\alpha\beta} (d_{i\alpha\uparrow}^\dagger d_{i\beta\downarrow}^\dagger d_{i\alpha\downarrow} d_{i\beta\uparrow} + d_{i\alpha\uparrow}^\dagger d_{i\alpha\downarrow}^\dagger d_{i\beta\downarrow} d_{i\beta\uparrow}) \end{aligned} \quad (5)$$

is the two-particle interaction term for  $3d$  electrons [28]. There are two independent parameters in this Hamiltonian, the Coulomb repulsion of electrons on the same orbital,  $U_0$ , and the average Hund's coupling,  $J_{\text{avg}} = \frac{1}{2l(2l+1)} \sum_{\alpha\neq\beta} J_{\alpha\beta}$ , with  $U_{\alpha\beta} = 3U_0\mathbb{1} - 2J_{\alpha\beta}$ . The explicit form of the interaction matrix  $J_{\alpha\beta}$  is given in Appendix B.

We first determine via *ab initio* methods the hopping parameters  $t_{i\alpha,j\beta}$  in Eq. (3) and then the spin-orbit coupling constant  $\lambda$  in Eq. (4). We perform nonmagnetic, nonrelativistic DFT calculations within an all-electron full-potential local orbital (FPLO) [29] basis and use for the exchange-correlation functional the generalized gradient approximation (GGA) [30]. The hopping parameters are then obtained from projective Wannier functions [31,32] as implemented in FPLO [33].

For the  $\text{Lu}_2\text{V}_2\text{O}_7$  pyrochlore, we use the experimental structure determined by Haghghirad *et al.* [34]. We show in Fig. 2 the total density of states, which is dominated by vanadium  $3d$  weights near the Fermi level. Because of the distorted oxygen octahedra surrounding each vanadium atom, illustrated in Fig. 1(b), there is a trigonal crystal field splitting of the  $d$  orbitals [see right panel of Fig. 2(c)]. This results in doubly degenerate  $d_{xy}$  and  $d_{x^2-y^2}$ , as well as  $d_{xz}$  and  $d_{yz}$  orbitals. Our choice of local coordinate systems at each vanadium ion is the same as the one used in Ref. [35]. The  $z$  axes point along the cubic  $\langle 111 \rangle$  directions, the  $x$  axes point along the cubic  $\langle 01\bar{1} \rangle$  directions while the  $y$  axes point along the  $\langle \bar{2}11 \rangle$  directions such that  $\langle xyz \rangle$  form a local orthogonal triad, as illustrated in Fig. 2(c). For a detailed description, we list in Appendix C the most relevant on-site (see Table III) and nearest-neighbor (see Table IV) hopping parameters.

Having determined  $t_{i\alpha,j\beta}$ , we next proceed to compute  $\lambda$ . We first derive the analytical expressions for the spin-orbit coupling matrix elements. The scalar product  $\vec{L} \cdot \vec{S} = \sum_{r_i} L_{r_i} S_{r_i}$  leads to a dependence on the direction of the local axes  $r_i = \{x_i, y_i, z_i\}$  at site  $i$ . The matrix elements can be evaluated using the Kronecker product,

$$\sum_{r_i} \langle i\alpha\sigma | (L_{r_i} S_{r_i}) | i\beta\sigma' \rangle = \sum_{r_i} \langle \alpha_i | L_{r_i} | \beta_i \rangle \otimes \langle \sigma | S_{r_i} | \sigma' \rangle, \quad (6)$$

where  $\alpha_i, \beta_i$  label the site-dependent  $d$  orbitals at site  $i$ . The spin operator  $S_{r_i}$  should have the components aligned along the local coordinate frame while the state  $|\sigma'\rangle = \{|\uparrow\rangle, |\downarrow\rangle\}$  is

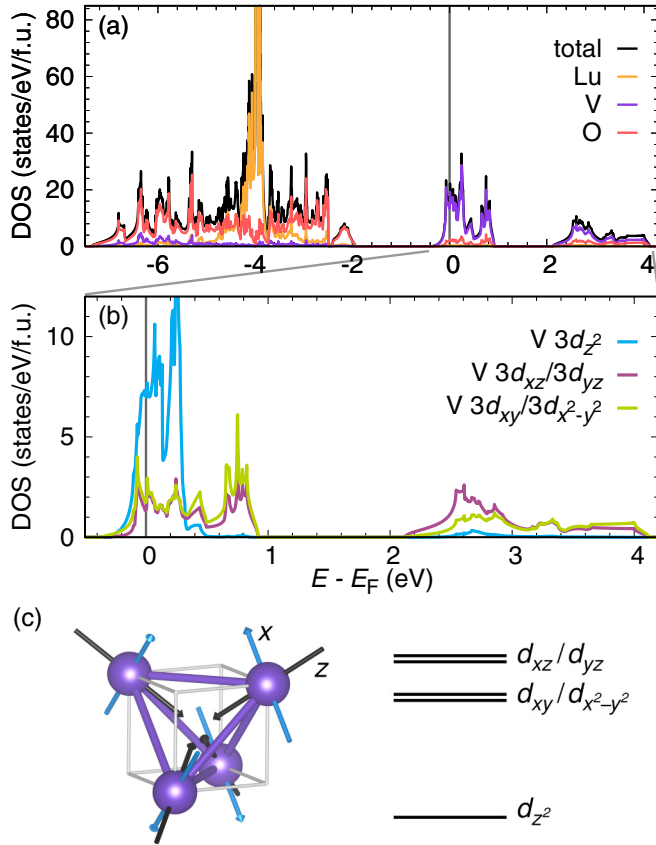


FIG. 2. (a) Nonrelativistic density of states (DOS) of  $\text{Lu}_2\text{V}_2\text{O}_7$  in the energy range  $[-7 \text{ eV}, 4 \text{ eV}]$  obtained in the GGA approximation. Shown are the total, as well as partial DOS corresponding to V, O, and Lu. (b) Vanadium orbital-resolved DOS around the Fermi level. (c) Illustration of the local reference frame in one tetrahedron of vanadium atoms, and orbital energy hierarchy in  $\text{Lu}_2\text{V}_2\text{O}_7$ .

defined in a global coordinate frame. We therefore have to rotate the spin operator in each local reference frame (see Fig. 3). For example, for site No. 1, the local  $z$  axis,  $\vec{z}_1$ ,

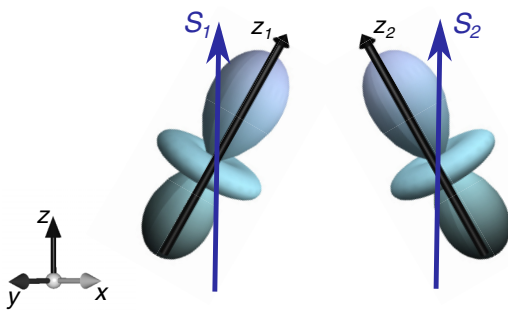


FIG. 3. Reference frames of spin and orbital degrees of freedom on two neighboring sites. The spins  $S_1, S_2$  are given in the global reference frame and the orbitals are  $d_{z^2}$  orbitals in the local reference frame at each site. Due to the site-dependent local coordinate frame, the spin operators have to be rotated in each local reference frame.

expressed in the global coordinate system is

$$\vec{z}_1 = \frac{1}{\sqrt{3}} \begin{pmatrix} 1 \\ 1 \\ 1 \end{pmatrix}.$$

Therefore, the spin operator measuring the local  $z$  component at this site is

$$S_{z_1} = \frac{1}{\sqrt{3}}(S_x + S_y + S_z),$$

where the spin operators are  $\vec{S} = \frac{1}{2}\vec{\sigma}$ , with  $\vec{\sigma}$  the Pauli matrices. On the other hand, the matrix elements of the angular momentum are evaluated at each vanadium local coordinate frame as given in Eq. (6).

By application of the Kronecker product in Eq. (6), the analytical expressions for the spin-orbit coupling matrix elements at every site are obtained, leaving only the spin-orbit coupling strength  $\lambda$  to be determined. Two main properties contribute to the value of  $\lambda$ : the nature of the ion (vanadium  $\text{V}^{4+}$  here) for which the spin-orbit interaction is being considered and, to a smaller degree, the crystal environment. In order to take into account these effects, we perform fully relativistic DFT calculations with FPLO and map via a numerical fitting procedure the sum of  $H_{\text{hop}}$  in Eq. (3) and  $H_{\text{SOC}}$  in Eq. (4), where  $H_{\text{hop}}$  contains the hopping parameters previously determined, to the relativistic DFT band structure. The only parameter left to fit the relativistic DFT band structure is then  $\lambda$ .

We illustrate this procedure in Fig. 4 for  $\text{Lu}_2\text{V}_2\text{O}_7$ . As expected, the spin-orbit coupling causes band splittings with respect to the nonrelativistic band structure: compare the tight-binding band structure represented by the purple curve (which reproduces well the nonrelativistic DFT band structure; not shown), with the fully relativistic band structure calculation, given by the blue curve in Fig. 4(c). Including the spin-orbit coupling contribution in the model Hamiltonian leads to a good representation of the relativistic band structure [red curve in Fig. 4(c)] from which we can extract  $\lambda$  through optimization. For  $\text{Lu}_2\text{V}_2\text{O}_7$ , we find  $\lambda \sim 30.0 \text{ meV}$ . As a reference, we note that the experimental value is  $\lambda_{\text{exp}} = 30.75 \text{ meV}$  for an isolated vanadium  $\text{V}^{4+}$  ion [36].

## B. Cluster diagonalization of $H_{\text{tot}}$

At this point, having determined from *ab initio* calculations  $t_{i\alpha, j\beta}$  and  $\lambda$ , we still need to choose the interaction parameters  $U_0$  and  $J_{\text{avg}}$  in  $H_{\text{int}}$ , given in Eq. (5). These two values will be left as model parameters and we will discuss them further below. Our aim here is to obtain a low-energy spin Hamiltonian out of the generalized Hubbard Hamiltonian  $H_{\text{tot}}$  Eq. (2). To this effect, we proceed with a cluster diagonalization of  $H_{\text{tot}}$ , focusing on the two-site case in the example of  $\text{Lu}_2\text{V}_2\text{O}_7$ .

We note the importance of the Hund's coupling for this multiorbital system. In  $\text{Lu}_2\text{V}_2\text{O}_7$ , the ground state is ferromagnetic [37]. The angle between two vanadium atoms and the nearest oxygen atom is  $\theta = 131.44^\circ$ . This is neither close to  $180^\circ$ , where according to the Goodenough-Kanamori rules antiferromagnetic coupling is favored, nor to  $90^\circ$ , which would lead to ferromagnetic coupling [38]. Miyahara *et al.* [39] suggested that ferromagnetism in  $\text{Lu}_2\text{V}_2\text{O}_7$  is induced by orbital ordering. These authors argue that the orbital or-

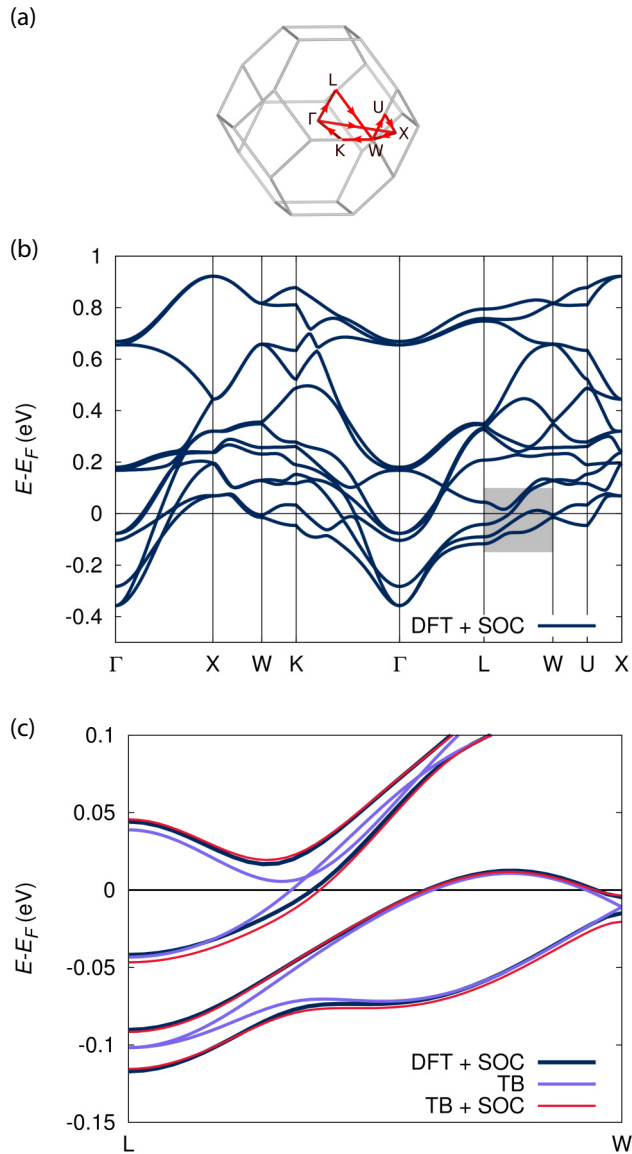


FIG. 4. (a) Chosen high-symmetry  $k$  path in the Brillouin zone of pyrochlore. (b) Relativistic band structure of  $\text{Lu}_2\text{V}_2\text{O}_7$  on the high-symmetry path. (c) Relativistic band structure between the high symmetry points L and W in a smaller energy window around the Fermi energy [gray shaded region in (b)]. The dark blue (DFT + SOC) curve is the result of the fully relativistic band structure calculation. The purple curve (TB) represents the tight-binding band structure from the nonrelativistic calculation. The red (TB + SOC) curve is the result of the tight-binding band structure taking the spin-orbit coupling term into account. The band splitting caused by relativistic effects is well reproduced, as can be seen by comparing the blue (DFT + SOC) and red (TB + SOC) curves.

dering in  $\text{Lu}_2\text{V}_2\text{O}_7$  leads to such a large ratio of hopping amplitudes  $t_{iz^2, jxy}/t_{iz^2, jz^2}$  and  $t_{iz^2, jx^2-y^2}/t_{iz^2, jz^2}$  that a ferromagnetic ground state is induced. This is of course only possible when a mechanism exists that favors ferromagnetic arrangements on different orbitals, the Hund's coupling. We note that the interaction part used in Ref. [39] is a simplified version of the correct  $3d$  Hubbard Hamiltonian [28]. Nevertheless, these arguments suggest that it is not possible to

neglect the various Hund's couplings,  $J_{\alpha\beta}$ , in the Hamiltonian and, at the same time, reproduce the correct ferromagnetic V-V exchange.

Notwithstanding the importance of considering the  $J_{\alpha\beta}$  couplings, there is a critical reason why all five V  $3d$  orbitals need to be included in the calculations. The oxygen octahedra surrounding the vanadium atoms are slightly distorted. This induces a trigonal crystal field splitting of the  $d$  orbitals (see Fig. 2), with the lowest level being nondegenerate. The necessity of including all five  $d$  orbitals is made evident by invoking simple perturbation-theory considerations. Specifically, the importance of the various states to the effective spin Hamiltonian that we aim to determine scales roughly with the inverse of the crystal field splitting. In a hypothetical case where the lowest orbitals were degenerate, these would play the main role in the physics of the system and it would be justified to consider only those. Otherwise, one has to take all orbitals into account. Furthermore, it is important to note that the difference of the magnetic quantum numbers of the lowest orbital  $d_{z^2}$  ( $m_l = 0$ ) with the next higher orbitals  $d_{xy}/d_{x^2-y^2}$  ( $m_l = \pm 2$ ) is two. As a result, the spin-orbit coupling  $\vec{L} \cdot \vec{S} = \frac{1}{2}(L_- S_+ + L_+ S_-) + L_z S_z$  has almost no contribution if we neglect the two highest-energy orbitals,  $d_{xz}/d_{yz}$  with  $m_l = \pm 1$  [see Fig. 2(c)].

$H_{\text{tot}}$  is diagonalized for two sites, five  $d$  orbitals and two spin degrees of freedom. The filling counting in  $\text{Lu}_2\text{V}_2\text{O}_7$  is one electron per V site so that we constrain the subspace to states containing two vanadium ions. In second quantization, the two-site/two-particle system has  $\binom{20}{2} = 190$  states, and we therefore need to diagonalize a  $190 \times 190$  matrix. Note that we have within this approach the constraint  $U_0 - 3J_{\alpha\beta} > 0$  for all orbitals; otherwise, states with two particles on a single site would become favorable because the system then gains energy with double occupation, and the projection onto singly occupied states is no longer justified.

In the following paragraphs, we investigate the properties of the four singly occupied states and their corresponding energy. We define the low-energy state  $|\psi\rangle$  via a linear combination of singly occupied states with coefficients  $c_{\sigma\sigma'}$  ( $\sigma = \uparrow, \downarrow$ )

$$|\psi\rangle = c_{\uparrow\uparrow} |\uparrow_{i,z^2} \uparrow_{j,z^2}\rangle + c_{\uparrow\downarrow} |\uparrow_{i,z^2} \downarrow_{j,z^2}\rangle + c_{\downarrow\uparrow} |\downarrow_{i,z^2} \uparrow_{j,z^2}\rangle + c_{\downarrow\downarrow} |\downarrow_{i,z^2} \downarrow_{j,z^2}\rangle, \quad (7)$$

where  $i, j$  are site indices.

We first discuss various limiting cases. In the nonrelativistic atomic limit ( $\lambda = 0$  and all hopping terms set to zero), the ground state is fourfold degenerate with every site being singly occupied with the electron located in the orbital of lowest energy; in  $\text{Lu}_2\text{V}_2\text{O}_7$  this is the  $d_{z^2}$  orbital. For two sites, the ground-state energy is then  $\varepsilon_0 = 2\varepsilon_{z^2}$ , which is twice the on-site energy of the  $d_{z^2}$  orbital.

If we switch on spin-orbit coupling, states with certain orbitals and spins get admixed, and the eigenenergies undergo a shift in the atomic limit. Henceforth, we deal with pseudo-orbitals  $\tilde{\alpha}$  with an energy for the lowest state  $\varepsilon_{\tilde{z}^2}^{\text{SO}}$ . The ground-state energy of the two-site system is then twice the on-site energy of the pseudo-orbital with the lowest energy  $\varepsilon_0^{\text{SO}} = 2\varepsilon_{\tilde{z}^2}^{\text{SO}}$ .

If we switch on hopping, but neglect spin-orbit coupling, we observe a triplet-singlet splitting in the energy spectrum and additional contributions from states that are not the low-energy states in the atomic limit are admixed. Without

TABLE I. Coefficients of the low-energy states in Lu<sub>2</sub>V<sub>2</sub>O<sub>7</sub>. Upper table: Without spin-orbit coupling, there are two energy levels, one of them triply degenerate with  $\varepsilon_0^{\text{hop}} = 0.43907$  eV, and a singlet with  $\varepsilon_1^{\text{hop}} = 0.44769$  eV. Lower table: Full Hamiltonian, there are four distinct energy levels.

$\varepsilon^{\text{hop}}$ (eV)	$c_{\uparrow\uparrow}$	$c_{\uparrow\downarrow}$	$c_{\downarrow\uparrow}$	$c_{\downarrow\downarrow}$
0.43907	1	0	0	0
0.43907	0	0	0	1
0.43907	0	0.70	0.70	0
0.44769	0	0.70	-0.70	0
$\varepsilon^{\text{SO+hop}}$ (eV)	$c_{\uparrow\uparrow}$	$c_{\uparrow\downarrow}$	$c_{\downarrow\uparrow}$	$c_{\downarrow\downarrow}$
0.43300	$0.69 - 0.06i$	0	0	$0.69 - 0.06i$
0.43306	$-0.47 + 0.15i$	$0.47 - 0.15i$	$0.47 - 0.15i$	$0.47 - 0.15i$
0.43307	$0.49 - 0.02i$	0.49	$0.49 - 0.05i$	$-0.49 - 0.02i$
0.44104	$0.02i$	$0.69 - 0.03i$	$-0.69 + 0.06i$	$0.02i$

the Hund’s couplings, antisymmetric states are energetically favored since the Pauli principle allows enhanced hopping processes in this case. The Hund’s coupling  $J_{\alpha\beta}$  represents a competing mechanism and can, depending on its strength, lead to the symmetric states being lowest in energy. Results for the energies  $\varepsilon^{\text{hop}}$  in Lu<sub>2</sub>V<sub>2</sub>O<sub>7</sub> are given in the upper Table I where we chose  $U_0 = 3.3$  eV and  $J_{\text{avg}} = 0.845$  eV.

By diagonalizing the full Hamiltonian, the mixing of orbitals and spins due to spin-orbit coupling combined with the orbital-dependent hoppings lead to an additional, very small splitting of the three lowest states for Lu<sub>2</sub>V<sub>2</sub>O<sub>7</sub> given by the energies  $\varepsilon^{\text{SO+hop}}$  in the lower Table I. In Lu<sub>2</sub>V<sub>2</sub>O<sub>7</sub> the lowest energies are between  $\varepsilon_0^{\text{SO+hop}} = 0.433$  eV and  $\varepsilon_4^{\text{SO+hop}} = 0.44104$  eV while the next higher eigenenergy (not shown) is  $\varepsilon_5^{\text{SO+hop}} = 0.59827$  eV. This energy gap leads to a well-defined separation of the low-energy states from the excited states, which allows us to focus on the low-energy states in the analysis below.

### C. Effective spin Hamiltonian

With the detailed information on the low-energy states of the two-site system now in hand, we construct an effective spin Hamiltonian acting within the low-energy subspace given by the four states described above. Within these four states, we neglect the very small coefficients of basis states, which do not describe singly occupied states in the low-energy orbital. In this way, we construct a basis that is not orthonormal,  $|b_j\rangle = \sum_i c_i |s_i\rangle$ , where  $|s_i\rangle$  are the four singly occupied low-energy states as in Eq. (7). The coefficients  $c_i$  are those of the lower table in Table I. The overlap matrix  $P$ , with elements  $P_{ij} \equiv c_i^* c_j \langle s_i | s_j \rangle$  for Lu<sub>2</sub>V<sub>2</sub>O<sub>7</sub>, is diagonal with overlaps around 0.96.

After orthonormalization [40], the coefficients  $c_i$  are slightly modified (shown in Table II) while the eigenvalues are unchanged. At this point of the calculation, the effective

Hamiltonian is given in the orthonormalized basis  $|b_j\rangle$ , with the coefficients given in Table II.

As an alternative approach for constructing the effective spin Hamiltonian, as well as a check for consistency, we also performed second-order perturbation theory and compared the resulting effective Hamiltonian with the one obtained via the cluster diagonalization. In second-order perturbation theory [41],  $H_{\text{eff}}^{\text{PT}} = \mathbb{P} H_{\text{hop}}^{i\neq j} \mathbb{R} H_{\text{hop}}^{i\neq j} \mathbb{P}$  up to two intersite hopping processes are considered. The operator  $\mathbb{P} = \sum_i |s_i\rangle \langle s_i|$  projects onto the low-energy subspace while  $\mathbb{R} = \sum_{ij} |e_i\rangle \langle e_i| (\varepsilon_0 - H_0)^{-1} |e_j\rangle \langle e_j|$  projects onto the renormalized subspace of excited states  $|e_i\rangle$ . The unperturbed Hamiltonian  $H_0$  contains the total Hamiltonian given in Eq. (2) except for the intersite hopping  $H_{\text{hop}}^{i\neq j}$ . In the limit  $U_0 \gg t_{i\alpha, j\beta}$ , we obtain, as it should be, the same results with both methods. In the region of physically relevant model parameters  $U_0$  and  $J_{\text{avg}}$ , there are nevertheless higher-order corrections to the second-order perturbation theory results.

We now use spin projectors to obtain the sought effective spin Hamiltonian.

#### Spin projectors

Using the Abrikosov pseudofermion representation for spin 1/2 operators,

$$c_{i\uparrow}^\dagger c_{i\downarrow} = S_i^+, \quad c_{i\downarrow}^\dagger c_{i\uparrow} = S_i^-,$$

$$c_{i\uparrow}^\dagger c_{i\uparrow} = \frac{1}{2} + S_i^z, \quad c_{i\downarrow}^\dagger c_{i\downarrow} = \frac{1}{2} - S_i^z,$$

and the fact that an operator in second quantization is expressed as

$$\hat{A} = \sum_{\mu\nu\mu'v'} \langle \mu\nu | \hat{A} | \mu'v' \rangle c_{1\mu}^\dagger c_{2\nu}^\dagger c_{2v'} c_{1\mu'},$$

we can translate an effective spin-1/2 Hamiltonian written in second quantization to a spin Hamiltonian. For example, the

TABLE II. Coefficients of the states in the orthonormal low energy for Lu<sub>2</sub>V<sub>2</sub>O<sub>7</sub>.

$\varepsilon$ (eV)	$c'_{\uparrow\uparrow}$	$c'_{\uparrow\downarrow}$	$c'_{\downarrow\uparrow}$	$c'_{\downarrow\downarrow}$
0.43300	$0.7043 - 0.0626i$	0	0	$0.7043 - 0.0626i$
0.43306	$-0.4758 + 0.1526i$	$0.4764 - 0.1529i$	$0.4764 - 0.1528i$	$0.4758 - 0.1526i$
0.43307	$-0.4995 + 0.0245i$	0.4999	$0.4975 + 0.0493i$	$-0.4995 - 0.0245i$
0.44104	$-0.0012 - 0.0175i$	$-0.7063 + 0.0295i$	$0.7039 - 0.0645i$	$0.0012 + 0.0175i$

operator

$$|\uparrow_{i,z^2}\uparrow_{j,z^2}\rangle\langle\uparrow_{i,z^2}\uparrow_{j,z^2}| = c_{i,z^2\uparrow}^\dagger c_{j,z^2\uparrow}^\dagger c_{j,z^2\uparrow} c_{i,z^2\uparrow}$$

leads to a term that couples the  $z$  components of the spin

$$c_{i,z^2\uparrow}^\dagger c_{j,z^2\uparrow}^\dagger c_{j,z^2\uparrow} c_{i,z^2\uparrow} = \left(\frac{1}{2} + S_i^z\right)\left(\frac{1}{2} + S_j^z\right).$$

Having introduced spin-1/2 operators, we can recast the relevant terms in the electronic Hamiltonian in the form of  $3 \times 3$  matrices that describe (anisotropic) interactions between the components of the spins 1/2 at sites  $i$  and  $j$ . The spin Hamiltonian then reads

$$H_{\text{spin}} = \vec{S}_i^T \Gamma_{ij} \vec{S}_j \quad (8)$$

where the bilinear spin-spin interaction matrix  $\Gamma_{ij}$  has components (see also Ref. [42])

$$\Gamma_{ij} = \begin{pmatrix} \mathcal{J}_{ij} + \mathcal{K}_{ij}^{xx} & \mathcal{D}_{ij}^z + \mathcal{K}_{ij}^{xy} & -\mathcal{D}_{ij}^y + \mathcal{K}_{ij}^{xz} \\ -\mathcal{D}_{ij}^z + \mathcal{K}_{ij}^{xy} & \mathcal{J}_{ij} + \mathcal{K}_{ij}^{yy} & \mathcal{D}_{ij}^x + \mathcal{K}_{ij}^{yz} \\ \mathcal{D}_{ij}^y + \mathcal{K}_{ij}^{xz} & -\mathcal{D}_{ij}^x + \mathcal{K}_{ij}^{yz} & \mathcal{J}_{ij} - \mathcal{K}_{ij}^{xx} - \mathcal{K}_{ij}^{yy} \end{pmatrix}. \quad (9)$$

The matrix consists of the Heisenberg exchange  $\mathcal{J}_{ij}$ , the Dzyaloshinskii-Moriya vector  $\vec{\mathcal{D}}_{ij}$  and the traceless symmetric tensor  $\hat{\mathcal{K}}_{ij}$ ; the spin Hamiltonian consequently has the form of Eq. (1). The symmetric tensor  $\hat{\mathcal{K}}_{ij}$  is chosen to be traceless to ensure that the definition of the Heisenberg exchange  $\mathcal{J}_{ij}$  is not modified by considering additional nonrotationally invariant terms.

We can now determine the values for the coupling parameters in Eq. (9) from the previously derived *ab initio* hopping parameters and  $\lambda$ . The details of the crystal structure, which influences the form of the exchange parameters, like the symmetry and the orbital hierarchy, are implicitly encoded in these *ab initio* parameters.

#### D. $\vec{\mathcal{D}}_{ij}$ and $\hat{\mathcal{K}}_{ij}$ in pyrochlore systems

Since  $H_{\text{spin}}$  in Eq. (8) ought to be invariant under the symmetry operations of the crystal, we analyze now the symmetries of the pyrochlore lattice. It is known from the Moriya rules [20] that the direction of the Dzyaloshinskii-Moriya vector  $\vec{\mathcal{D}}_{ij}$  depends on the orientation of the mirror planes as well as rotation axes in the system considered. In fact, these symmetries also determine the number of independent parameters in the symmetric tensor  $\hat{\mathcal{K}}_{ij}$ .

For simplicity, let us assume that one bond between sites A and B is in the direction of the global  $x$  axis, as shown in Fig. 5(a). In the pyrochlore lattice, there are two mirror planes, which are important for the determination of the symmetry properties of the exchange parameters.

One mirror plane is perpendicular to A-B and passes through C. Since spin is a pseudovector, it transforms under this symmetry operation as

$$\begin{pmatrix} S_A^x \\ S_A^y \\ S_A^z \end{pmatrix} \rightarrow \begin{pmatrix} S_B^x \\ -S_B^y \\ -S_B^z \end{pmatrix} \quad \text{and} \quad \begin{pmatrix} S_B^x \\ S_B^y \\ S_B^z \end{pmatrix} \rightarrow \begin{pmatrix} S_A^x \\ -S_A^y \\ -S_A^z \end{pmatrix},$$

with the spin Hamiltonian necessarily invariant under this symmetry operation. Therefore, those terms in the Hamiltonian for

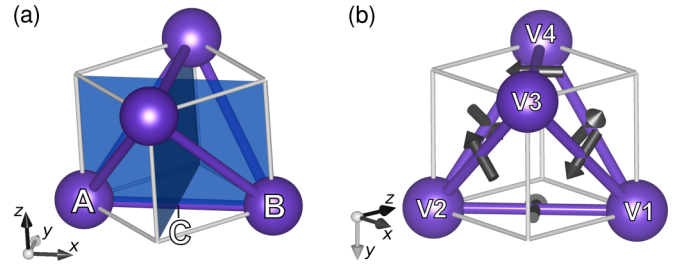


FIG. 5. (a) Vanadium tetrahedron showing the two mutually perpendicular mirror planes relevant to the A-B bond. One plane includes the bond A-B, while the other bisects this bond at C. The presence of such mirror planes constrains the form of the local DM vectors and symmetric tensors. (b) Direction of the Dzyaloshinskii-Moriya vectors in a pyrochlore system in the global coordinate system considered in the calculations.

which the sign is changed under such mirror reflection have to vanish,

$$\mathcal{D}_{AB}^x = 0, \quad \mathcal{K}_{AB}^{xy} = 0, \quad \mathcal{K}_{AB}^{xz} = 0.$$

The second mirror plane includes A-B and lies in the  $xz$  plane for the chosen global coordinate system. With the symmetry operations

$$\begin{pmatrix} S_A^x \\ S_A^y \\ S_A^z \end{pmatrix} \rightarrow \begin{pmatrix} -S_B^x \\ S_B^y \\ -S_B^z \end{pmatrix} \quad \text{and} \quad \begin{pmatrix} S_B^x \\ S_B^y \\ S_B^z \end{pmatrix} \rightarrow \begin{pmatrix} -S_A^x \\ S_A^y \\ -S_A^z \end{pmatrix},$$

one finds the restrictions

$$\mathcal{D}_{AB}^x = 0, \quad \mathcal{D}_{AB}^z = 0, \quad \mathcal{K}_{AB}^{xy} = 0, \quad \mathcal{K}_{AB}^{yz} = 0.$$

In conclusion, the direction of the Dzyaloshinskii-Moriya vector is, except for its sign, fully determined by symmetry considerations. Its only nonvanishing contribution is in the global  $y$  direction, perpendicular to the bond under consideration and within the face of the cube enclosing the tetrahedron. The symmetric tensor is diagonal for this choice of coordinate system. We thus have

$$\vec{\mathcal{D}}_{AB} = \begin{pmatrix} 0 \\ \mathcal{D}_{AB}^y \\ 0 \end{pmatrix}, \quad \hat{\mathcal{K}}_{AB} = \begin{pmatrix} \mathcal{K}_{AB}^{xx} & 0 & 0 \\ 0 & \mathcal{K}_{AB}^{yy} & 0 \\ 0 & 0 & -\mathcal{K}_{AB}^{xx} - \mathcal{K}_{AB}^{yy} \end{pmatrix}.$$

Hence, for the pyrochlore system with only nearest-neighbor interactions, there is only one independent exchange parameter for the Dzyaloshinskii-Moriya vector and there are two independent parameters that characterize the symmetric tensor  $\hat{\mathcal{K}}_{ij}$ .

In our calculations, we worked in a global coordinate system aligned along the cubes edges. We show in Fig. 5(b) all the DM vectors for one tetrahedron, with their explicit form given in Appendix D in this global coordinate system. To find the correct contributions to both the DM vector and the symmetric tensor  $\hat{\mathcal{K}}$  within this description, one has to rotate the coordinate system used above.

As an example, we give the result for the bond 1-2, as defined in Fig. 5(b), which is obtained by a rotation of  $\pi/4$

about the  $z$  axis and a rotation of  $\pi/2$  about the  $x$  axis

$$\vec{D}_{12} = \begin{pmatrix} -\mathcal{D}_{12}^x \\ 0 \\ -\mathcal{D}_{12}^x \end{pmatrix}, \quad \hat{\mathcal{K}}_{12} = \begin{pmatrix} \mathcal{K}_{12}^{xx} & 0 & \mathcal{K}_{12}^{xz} \\ 0 & -2\mathcal{K}_{12}^{xx} & 0 \\ \mathcal{K}_{12}^{xz} & 0 & \mathcal{K}_{12}^{xx} \end{pmatrix},$$

with  $\mathcal{K}_{12}^{xx} = \frac{1}{2}(\mathcal{K}_{AB}^{xx} + \mathcal{K}_{AB}^{yy})$ ,  $\mathcal{K}_{12}^{yy} = \frac{1}{2}(\mathcal{K}_{AB}^{xx} - \mathcal{K}_{AB}^{yy})$ , and  $\mathcal{D}_{12}^x = \frac{\mathcal{D}_{AB}^y}{\sqrt{2}}$ .

As previously noted for odd electron ions in pyrochlore systems [35], we therefore have, together with the isotropic Heisenberg exchange  $\mathcal{J}_{12}$ , four independent bilinear spin-spin couplings, in principle [43]. We discuss in Appendix A various representations of equivalent spin Hamiltonians using different spin quantization frames.

The dependence of the energy parameters in the spin Hamiltonian on the model parameters  $U_0$  and  $J_{\text{avg}}$  in  $\text{Lu}_2\text{V}_2\text{O}_7$  is shown in Fig. 6. The Hund’s coupling within  $3d$  orbitals [38] is estimated to be 0.8–0.9 eV. For the Coulomb repulsion  $U_0$  on the same orbital on  $\text{V}^{4+}$  ions, we considered values between 3 and 4 eV.

With the parameter choice  $U_0 = 3.3$  eV and  $J_{\text{avg}} = 0.845$  eV, we extract from the effective Hamiltonian (coefficients given in Table II) the following energy parameters (all in meV)

$$\mathcal{J}_{12} = -7.99, \quad \vec{D}_{12} = \begin{pmatrix} -0.4 \\ 0 \\ 0.4 \end{pmatrix},$$

$$\hat{\mathcal{K}}_{12} = \begin{pmatrix} -0.05 & 0 & 0.02 \\ 0 & 0.1 & 0 \\ 0.02 & 0 & -0.05 \end{pmatrix}. \quad (10)$$

The isotropic Heisenberg exchange  $\mathcal{J}_{12}$  is ferromagnetic and in reasonably good agreement with the experimental value  $\mathcal{J} = -8.22$  meV in Ref. [25], and not too far off from the results obtained from *ab initio* calculations with the “energy mapping method” of Ref. [26] ( $\mathcal{J} = -7.09$  meV). We focus on a choice of interaction parameters, based on the agreement of the Heisenberg exchange with the inelastic neutron scattering experiment [25], so that our calculated values for the Dzyaloshinskii-Moriya interaction and the symmetric tensor can be more easily compared with the experimental results.

As explained above and as illustrated in Fig. 5(b), the directions of the  $\vec{D}_{ij}$  vectors are fully determined by symmetry considerations [19,20], with only its sign depending on microscopic atomic details. The numerical results completely agree with the prediction of Moriya’s rules, which confirms that the choice of local coordinate systems and the rotations performed throughout our calculations implement the crystal symmetry correctly. The orientation of the DM vectors that we find here corresponds to the so-called indirect case of Ref. [19]. The ratio

$$\frac{|\vec{D}|}{|\mathcal{J}|} \approx 0.07, \quad (11)$$

where  $|\vec{D}|$  is calculated as  $\sqrt{\mathcal{D}_x^2 + \mathcal{D}_y^2 + \mathcal{D}_z^2}$ , is lower than the two experimental results [18,25] for this material. By fitting transport data, Ref. [18] determined  $|\vec{D}|/\mathcal{J} \simeq 0.32$ , while the ratio obtained from inelastic neutron scattering [25] is  $|\vec{D}|/\mathcal{J} \simeq 0.18$ . The theoretical approach of Xiang *et al.* [26] using differences of DFT total energies for various spin

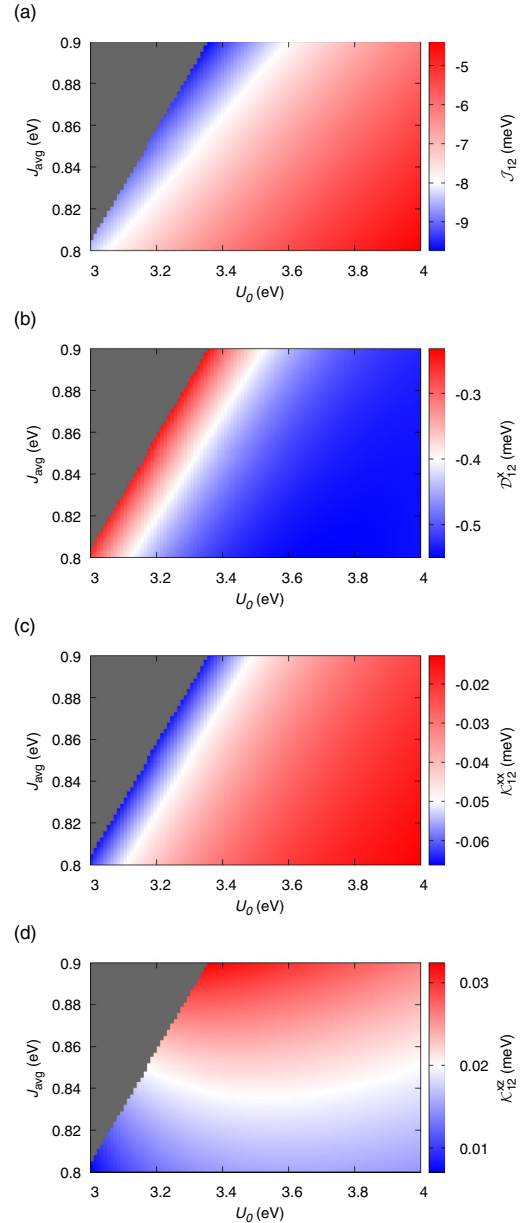


FIG. 6. Dependence of the calculated exchange parameters on the interaction parameters  $U_0$  and  $J_{\text{avg}}$ . The results for a certain choice of interaction parameters are given in Eq. (10). The gray area far left is the forbidden region where, for  $U_0 - 3J_{\text{avg}} < 0$ , the projection on singly occupied states is no longer justified and the white lines correspond to the theoretical results given in Eq. (10). (a) Heisenberg exchange  $\mathcal{J}_{12}$ . For comparison, experiment [25] estimates  $|\mathcal{J}| = 8.22$  meV. (b)  $\mathcal{D}_{12}^x$ , given in the global coordinate system as in Fig. 5(b). The results are below the experimental estimates, which correspond to  $\mathcal{D}_{12}^x = -0.8$  meV [18] and  $\mathcal{D}_{12}^x = -1.05$  meV [25]. Note, that we are reporting  $\mathcal{D}_{12}^x$  and not  $|\vec{D}_{12}| = \sqrt{2}|\mathcal{D}_{12}^x|$ . (c), (d) Independent contributions to the symmetric anisotropic exchange  $\hat{\mathcal{K}}$ . The calculated values are for none of the interaction parameters  $U_0$ ,  $J_{\text{avg}}$  small enough to neglect them.

configurations determined a smaller ratio of  $|\vec{D}|/\mathcal{J} \simeq 0.048$ . We discuss possible reasons for the large difference between these two values in Sec. III.

The symmetric tensor results in smaller corrections to the nearest-neighbor Heisenberg spin Hamiltonian, though these are not entirely negligible when compared to  $|\vec{D}|/|\mathcal{J}|$  in Eq. (11), with

$$\frac{|\hat{\mathcal{K}}|}{|\mathcal{J}|} = 0.02,$$

where  $|\hat{\mathcal{K}}|$  is the Frobenius norm of the symmetric tensor.

### III. SUMMARY

In summary, we presented a method to determine the spin exchange parameters of a spin-1/2 system combining nonrelativistic and relativistic *ab initio* density functional theory (DFT) calculations with exact diagonalization of a generalized Hubbard model on a finite cluster. Projecting the Hamiltonian onto the low-energy subspace and using spin projectors, we transformed the effective Hamiltonian into a spin Hamiltonian, considering all allowed isotropic and anisotropic nearest-neighbor bilinear exchange parameters for a spin-1/2 system. Using this formalism, we determined for  $\text{Lu}_2\text{V}_2\text{O}_7$  the four independent exchange parameters for a certain choice of Hubbard repulsion  $U_0$  and Hund's coupling  $J_{\text{avg}}$ .

The isotropic (Heisenberg) exchange parameter  $\mathcal{J}_{ij}$  that we determined,  $\mathcal{J}_{ij} \approx -8 \text{ meV}$ , is close to the experimental value ( $\mathcal{J}_{ij} \approx -8.22 \text{ meV}$ ) extracted from inelastic neutron scattering (INS) data [25]. On the other hand, the ratio of the Dzyaloshinskii-Moriya interaction to the Heisenberg exchange in Eq. (11) is almost a factor 3 smaller than the  $|\vec{D}_{ij}|/|\mathcal{J}_{ij}| \simeq 0.18$  obtained from the same INS data. As such, the discrepancy between the present calculations and the  $|\vec{D}_{ij}|/|\mathcal{J}_{ij}|$  value extracted from INS appears rather large, perhaps at the verge of suggesting a paradox as per the spin-spin interaction parameters of this material. We comment further on that below. We note that the  $\mathcal{J}_{ij} \approx -3.4 \text{ meV}$  value found by fitting the magnetic specific heat [24] in Ref. [18] is significantly different from both the INS value and the present DFT result. This may suggest a necessity to reinvestigate the low-temperature magnetic specific heat data of this compound as well as reanalyzing it. In the same vein, the  $|\vec{D}_{ij}|/|\mathcal{J}_{ij}| \simeq 1/3$  determined by fitting transport data [18] is significantly larger than both the present DFT ratio [Eq. (11)] and the INS results [25]. It is unclear to what extent this surprisingly large ratio for a 3d transition metal ion ( $\text{V}^{4+}$ ) results from the small  $\mathcal{J}_{ij} \approx -3.4 \text{ meV}$  found from specific heat [18,24]. As the INS data directly determines the spin stiffness, there appears to be no simple way in which the magnetic specific heat value  $\mathcal{J}_{ij} \approx -3.4 \text{ meV}$  could be reconciled with the  $\mathcal{J}_{ij} \approx -8.22 \text{ meV}$  value that parameterizes the spin stiffness directly probed by INS.

Returning to the aforementioned difference between the INS and DFT  $|\vec{D}_{ij}|/|\mathcal{J}_{ij}|$  ratios, a few comments are in order. First of all, the fit to the INS data considered only nearest-neighbor exchange and Dzyaloshinskii-Moriya interactions, ignoring symmetric anisotropic exchange (the two components of  $\hat{\mathcal{K}}_{ij}$ ) as well as any interaction beyond nearest neighbors. Incorporating those in the fitting could lead to a renormalization of the  $|\vec{D}_{ij}|/|\mathcal{J}_{ij}|$  ratio. This is due to the fact that the spin stiffness, determined through the quadratic

momentum dependence of the magnon dispersion near the zone center [25], would no longer solely, and uniquely, fix  $\mathcal{J}_{ij}$ . It may also be worthwhile to explore the effect of the subleading anisotropic components ( $\hat{\mathcal{K}}_{ij}$ ) on the dispersion. Similarly, we only considered (two-site) nearest-neighbor interactions in our calculations and, as such, the accuracy of our exchange parameters are also hampered by the same distance truncation of the spin Hamiltonian used in the INS data analysis.

Regarding the comparison of our results with the theoretical results reported in Ref. [26] we find that the value of the isotropic nearest-neighbor Heisenberg exchange interaction is similar in both calculations. This is not surprising since both calculations originate from an initial DFT analysis. Reference [26] uses total DFT energy differences for various spin configurations and maps them to an extended Heisenberg model. We, on the other hand, take the DFT results for the determined hopping parameters and project a generalized Hubbard model with these hopping matrix elements to an extended Heisenberg model. As the nearest-neighbor Heisenberg exchange interaction is the largest energy scale in the problem, differences between the results of both methods should be reasonably small for this interaction.

However, the two calculations differ significantly on the choice of the mapping spin Hamiltonian and this has important consequences for the rest of the parameter estimates. We consider the most general spin Hamiltonian describing a quantum spin-1/2 system restricted to nearest-neighbor interactions. Reference [26] focuses on a spin Hamiltonian that does not include contributions from the symmetric part of the anisotropic exchange. A notable result of our work is that these terms are not entirely negligible in  $\text{Lu}_2\text{V}_2\text{O}_7$ . Furthermore, the authors of Ref. [26] include a single-ion anisotropy term of the form  $-B(S_z)^2$  in their parametric spin Hamiltonian which, in a quantum mechanical description of a spin-1/2 system, is a trivial constant as the square of all four Pauli matrices is twice the  $2 \times 2$  identity matrix. This suggests that there may exist a risk of confusion when parameterizing polarized (classical) magnetic moment configurations within DFT ultimately represented by quantum spin-1/2 degrees of freedom. To avoid such a risk, we chose to strictly stay within a quantum mechanical description of the spin Hamiltonian where the single-ion anisotropy term is absent at the very outset. Such considerations explain the differences between the results of the two theoretical approaches; (i) the Dzyaloshinskii-Moriya interaction is in our calculation a factor of 1.5 larger than that of Ref. [26]; (ii) we find a nonzero symmetric anisotropic term and (iii) there is, by construction, no single-ion anisotropy term in our case. Furthermore, we note that the calculations in Ref. [26] have been performed for  $\text{Y}_2\text{V}_2\text{O}_7$  instead of  $\text{Lu}_2\text{V}_2\text{O}_7$ , which may also result in (small) differences in the exchange parameters.

At first sight, it would naively appear that the insulating  $\text{Lu}_2\text{V}_2\text{O}_7$  pyrochlore, with its ferromagnetic ground state and a transition temperature of  $T_c \approx 70 \text{ K}$ , should be a textbook example of spin-1/2 ferromagnetism on a non-Bravais lattice well described by isotropic Heisenberg exchange with leading anisotropic exchange perturbations in the form of Dzyaloshinskii-Moriya (DM) interactions. However, at the present time, there appears to be some significant discrepancy between the scale of the DM interaction determined from

transport measurements [18], inelastic neutron scattering data [25] and from our density functional theory calculations. It would certainly be comforting, in terms of one's understanding of what would appear as simple ferromagnetism of localized moments, to resolve this disagreement. Furthermore, in view of the interests in topological aspects of magnon excitations induced by antisymmetric spin-spin interactions [18,22,23], a definite progress in obtaining a quantitative global understanding of the magnetic properties of Lu<sub>2</sub>V<sub>2</sub>O<sub>7</sub> would be useful.

#### ACKNOWLEDGMENTS

The authors acknowledge fruitful discussions with Steffen Backes, Vladislav Borisov, Zhihao Hao, Claudine Lacroix, Paul McClarty, Jeff Rau, Igor Solovyev, Julian Stobbe, Igor Mazin, Stephen Winter, and Alexander Yaresko. The work at Frankfurt University was supported by the Deutsche Forschungsgemeinschaft (DFG) through project SFB/TRR49. The work at the University of Waterloo was supported by the NSERC of Canada, the Canada Research Chair program (M.J.P.G., Tier 1). This research was also supported in part by the Perimeter Institute for Theoretical Physics. Research at the Perimeter Institute is supported by the Government of Canada through Innovation, Science and Economic Development Canada and by the Province of Ontario through the Ministry of Research, Innovation and Science.

#### APPENDIX A: CHOICE OF SPIN HAMILTONIAN REPRESENTATION

We discuss here the various representations of the generalized bilinear anisotropic Hamiltonian for spins 1/2 on the pyrochlore lattice. At least three different ways to parametrize the nearest-neighbor spin Hamiltonian have been employed.

In our study, we have used Eq. (1), which, due to its general form, is not limited to the description of pyrochlores, but applicable to any other crystal symmetry. However, as it does not explicitly expose the relevant symmetries of the specific system considered, it has the disadvantage that it seems to have more free parameters than there actually are. Consequently, one has to introduce additional symmetry considerations such as those presented in Sec. II D.

A more specific choice of parametrization for the case of pyrochlores was used by Thompson *et al.* [45] with four different nearest-neighbor bilinear exchange interactions

$$H_{\text{ex}} = H_{\text{Ising}} + H_{\text{iso}} + H_{\text{pd}} + H_{\text{DM}}. \quad (\text{A1})$$

It contains an Ising-like term with the spin projection on the local  $z$  axes on the site respectively

$$H_{\text{Ising}} = -\mathcal{J}_{\text{Ising}} \sum_{\langle ij \rangle} (\vec{S}_i \cdot \hat{z}_i)(\vec{S}_j \cdot \hat{z}_j), \quad (\text{A2})$$

an isotropic term, which has Heisenberg character,

$$H_{\text{iso}} = -\mathcal{J}_{\text{iso}} \sum_{\langle ij \rangle} \vec{S}_i \cdot \vec{S}_j, \quad (\text{A3})$$

a pseudodipolar term with projection on the bond  $\hat{r}_{ij}$  connecting site  $i$  and  $j$ ,

$$H_{\text{pd}} = -\mathcal{J}_{\text{pd}} \sum_{\langle ij \rangle} [\vec{S}_i \cdot \vec{S}_j - 3(\vec{S}_i \cdot \hat{r}_{ij})(\vec{S}_j \cdot \hat{r}_{ij})], \quad (\text{A4})$$

and a term which was labeled as the Dzyaloshinskii-Moriya term

$$H_{\text{DM}} = -\mathcal{J}_{\text{DM}} \vec{\Omega}_{\text{DM}}^{ij} \cdot (\vec{S}_i \times \vec{S}_j). \quad (\text{A5})$$

This way of parametrization includes only four different exchange parameters and is therefore convenient to describe a pyrochlore system, as shown in Sec. II D. By introducing the Ising-like term, there are additional contributions of the Dzyaloshinskii-Moriya term,  $|\vec{D}_{ij}| = -\mathcal{J}_{\text{DM}}^{ij} - \frac{\sqrt{2}}{3} \mathcal{J}_{\text{Ising}}^{ij}$ , so that  $\mathcal{J}_{\text{DM}}^{ij}$  and  $|\vec{D}_{ij}|$  describe the strength of different exchange processes. For the bond 1-2, the relation between parameterizations is

$$\mathcal{J}_{\text{Ising}}^{12} = 9\mathcal{K}_{12}^{xx} - 3\mathcal{K}_{12}^{xz}, \quad (\text{A6})$$

$$\mathcal{J}_{\text{iso}}^{12} = -\mathcal{J}_{12} + \mathcal{K}_{12}^{xx} - \frac{1}{3}\mathcal{K}_{12}^{xz}, \quad (\text{A7})$$

$$\mathcal{J}_{\text{pd}}^{12} = -2\mathcal{K}_{12}^{xx} + \frac{4}{3}\mathcal{K}_{12}^{xz}, \quad (\text{A8})$$

$$\mathcal{J}_{\text{DM}}^{12} = -|\vec{D}_{12}| - 3\sqrt{2}\mathcal{K}_{12}^{xx} + \sqrt{2}\mathcal{K}_{12}^{xz}. \quad (\text{A9})$$

The relation for the other bonds can be obtained by considering the pyrochlore symmetry.

Moreover, there is a third popular way of parametrization, introduced in Ref. [35], which, in an appendix, already pointed out the difference with the formalism used in Ref. [45]. In Eq. (2) of Ref. [35], the parameter matrix is explicitly given for a bond, which corresponds to bond 1-3 in Fig. 5(b),

$$\mathcal{J}_{\text{par}} = \begin{pmatrix} \mathcal{J}_2 & \mathcal{J}_4 & \mathcal{J}_4 \\ -\mathcal{J}_4 & \mathcal{J}_1 & \mathcal{J}_3 \\ -\mathcal{J}_4 & \mathcal{J}_3 & \mathcal{J}_1 \end{pmatrix}. \quad (\text{A10})$$

This leads to a modification of the Heisenberg exchange used in our notation and a renormalization of the Dzyaloshinskii-Moriya parameter,

$$\mathcal{J}_1 = \mathcal{J}_{13} - \frac{1}{2}\mathcal{K}_{13}^{xx}, \quad (\text{A11})$$

$$\mathcal{J}_2 = \mathcal{J}_{13} + \mathcal{K}_{13}^{xx}, \quad (\text{A12})$$

$$\mathcal{J}_3 = \mathcal{K}_{13}^{yz}, \quad (\text{A13})$$

$$\mathcal{J}_4 = -\frac{1}{\sqrt{2}}|\vec{D}_{13}|. \quad (\text{A14})$$

#### APPENDIX B: INTERACTION PARAMETERS IN $H_{\text{int}}$

We use the definition for the orbital-dependent Coulomb repulsion as used in Ref. [28],

$J_{\alpha\beta}$	$ d_{x^2-y^2}\rangle$	$ d_{z^2}\rangle$	$ d_{xy}\rangle$	$ d_{yz}\rangle$	$ d_{xz}\rangle$
$ d_{x^2-y^2}\rangle$	$U_0$	$j_2$	$j_3$	$j_1$	$j_1$
$ d_{z^2}\rangle$	$j_2$	$U_0$	$j_2$	$j_4$	$j_4$
$ d_{xy}\rangle$	$j_3$	$j_2$	$U_0$	$j_1$	$j_1$
$ d_{yz}\rangle$	$j_1$	$j_4$	$j_1$	$U_0$	$j_1$
$ d_{xz}\rangle$	$j_1$	$j_4$	$j_1$	$j_1$	$U_0$

The interaction parameters  $j_n$  can be expressed in terms of the Slater integrals [44]  $F_k$  as follows [28]:

$$j_1 = \frac{3}{49}F_2 + \frac{20}{9}\frac{1}{49}F_4 \quad (\text{B1})$$

$$j_2 = -2J_{\text{avg}} + 3j_1 \quad (\text{B2})$$

$$j_3 = 6J_{\text{avg}} - 5j_1 \quad (\text{B3})$$

$$j_4 = 4J_{\text{avg}} - 3j_1, \quad (\text{B4})$$

and where

$$U_0 = F_0 + \frac{8}{5}J_{\text{avg}}, \quad \text{and} \quad J_{\text{avg}} = \frac{5}{7}\frac{(F_2 + F_4)}{14}, \quad (\text{B5})$$

with  $F_4 = \frac{5}{8}F_2$ . In this work, we choose as independent parameters  $U_0$  and  $J_{\text{avg}}$ . The Coulomb repulsion matrix used in the interaction Hamiltonian (5) can be easily constructed as  $U_{\alpha\beta} = 3U_0\mathbb{1} - 2J_{\alpha\beta}$ .

### APPENDIX C: LOCAL COORDINATE SYSTEM

For a unit cell with the vanadium positions as follows (used within our calculations with full-potential local orbital (FPLO) basis),

$$\begin{aligned} \vec{v}_1 &= \begin{pmatrix} 1/2 \\ 1/2 \\ 1/2 \end{pmatrix}, & \vec{v}_2 &= \begin{pmatrix} 1/4 \\ 1/2 \\ 1/4 \end{pmatrix}, \\ \vec{v}_3 &= \begin{pmatrix} 1/2 \\ 1/4 \\ 1/4 \end{pmatrix}, & \vec{v}_4 &= \begin{pmatrix} 1/4 \\ 1/4 \\ 1/2 \end{pmatrix}. \end{aligned} \quad (\text{C1})$$

we use the local coordinate systems

$$\begin{aligned} \vec{x}_1 &= \frac{1}{\sqrt{2}}\begin{pmatrix} 0 \\ 1 \\ -1 \end{pmatrix}, & \vec{y}_1 &= \frac{1}{\sqrt{6}}\begin{pmatrix} -2 \\ 1 \\ 1 \end{pmatrix}, & \vec{z}_1 &= \frac{1}{\sqrt{3}}\begin{pmatrix} 1 \\ 1 \\ 1 \end{pmatrix}, \\ \vec{x}_2 &= \frac{1}{\sqrt{2}}\begin{pmatrix} 0 \\ 1 \\ 1 \end{pmatrix}, & \vec{y}_2 &= \frac{1}{\sqrt{6}}\begin{pmatrix} 2 \\ 1 \\ -1 \end{pmatrix}, & \vec{z}_2 &= \frac{1}{\sqrt{3}}\begin{pmatrix} -1 \\ 1 \\ -1 \end{pmatrix}, \\ \vec{x}_3 &= \frac{1}{\sqrt{2}}\begin{pmatrix} 0 \\ -1 \\ 1 \end{pmatrix}, & \vec{y}_3 &= \frac{1}{\sqrt{6}}\begin{pmatrix} -2 \\ -1 \\ -1 \end{pmatrix}, & \vec{z}_3 &= \frac{1}{\sqrt{3}}\begin{pmatrix} 1 \\ -1 \\ -1 \end{pmatrix}, \\ \vec{x}_4 &= \frac{1}{\sqrt{2}}\begin{pmatrix} 0 \\ -1 \\ -1 \end{pmatrix}, & \vec{y}_4 &= \frac{1}{\sqrt{6}}\begin{pmatrix} 2 \\ -1 \\ 1 \end{pmatrix}, & \vec{z}_4 &= \frac{1}{\sqrt{3}}\begin{pmatrix} -1 \\ -1 \\ 1 \end{pmatrix}. \end{aligned}$$

Within these local coordinate systems and for the vanadium atoms at the given positions, we obtain on-site energies as given in Table III, the most important hopping parameter between nearest neighbors are given in Table IV.

TABLE III. On-site energies  $t_{1\alpha,1\beta}$  (in eV) on vanadium site No. 1, the other three vanadium ions are symmetry equivalent.

	V1 $d_{x^2-y^2}$	V1 $d_{z^2}$	V1 $d_{xy}$	V1 $d_{yz}$	V1 $d_{xz}$
V1 $d_{x^2-y^2}$	1.5815	0	0	-1.2612	0
V1 $d_{z^2}$	0	0.2351	0	0	0
V1 $d_{xy}$	0	0	1.5815	0	-1.2612
V1 $d_{yz}$	-1.2612	0	0	1.8316	0
V1 $d_{xz}$	0	0	-1.2612	0	1.8316

### APPENDIX D: DIRECTION OF DZVALOSHINSKII-MORIYA VECTORS

For a primitive unit cell with the basis coordinates as in Eq. (C1), we have for the direction of the DM vectors

$$\begin{aligned} \hat{d}_{12} &= \frac{1}{\sqrt{2}}\begin{pmatrix} -1 \\ 0 \\ 1 \end{pmatrix}, & \hat{d}_{13} &= \frac{1}{\sqrt{2}}\begin{pmatrix} 0 \\ 1 \\ -1 \end{pmatrix}, \\ \hat{d}_{14} &= \frac{1}{\sqrt{2}}\begin{pmatrix} 1 \\ -1 \\ 0 \end{pmatrix}, & \hat{d}_{23} &= \frac{1}{\sqrt{2}}\begin{pmatrix} -1 \\ -1 \\ 0 \end{pmatrix}, \\ \hat{d}_{24} &= \frac{1}{\sqrt{2}}\begin{pmatrix} 0 \\ 1 \\ 1 \end{pmatrix}, & \hat{d}_{34} &= \frac{1}{\sqrt{2}}\begin{pmatrix} -1 \\ 0 \\ -1 \end{pmatrix}. \end{aligned} \quad (\text{D1})$$

This corresponds to the indirect case discussed in Ref. [19].

TABLE IV. Dominant hopping parameters  $t_{1\alpha,j\beta}$  (in eV) between nearest neighbors always with respect to vanadium site No. 1, the other hopping parameters result from symmetry operations.

	V2 $d_{x^2-y^2}$	V2 $d_{z^2}$	V2 $d_{xy}$	V2 $d_{yz}$	V2 $d_{xz}$
V1 $d_{x^2-y^2}$	-0.1384	0.0710	-0.0916	-0.0088	0.1113
V1 $d_{z^2}$	0.0710	-0.0421	0.1229	-0.0869	-0.1506
V1 $d_{xy}$	-0.0916	0.1229	-0.2441	0.1113	0.1198
V1 $d_{yz}$	-0.0088	-0.0869	0.1113	-0.0348	0.0383
V1 $d_{xz}$	0.1113	-0.1506	0.1198	0.0383	0.0093
	V3 $d_{x^2-y^2}$	V3 $d_{z^2}$	V3 $d_{xy}$	V3 $d_{yz}$	V3 $d_{xz}$
V1 $d_{x^2-y^2}$	-0.2970	-0.1419	0	0.1840	0
V1 $d_{z^2}$	-0.1419	-0.0421	0	0.1738	0
V1 $d_{xy}$	0	0	-0.0855	0	-0.0731
V1 $d_{yz}$	0.1840	0.1738	0	0.0314	0
V1 $d_{xz}$	0	0	-0.0731	0	-0.0569
	V4 $d_{x^2-y^2}$	V4 $d_{z^2}$	V4 $d_{xy}$	V4 $d_{yz}$	V4 $d_{xz}$
V1 $d_{x^2-y^2}$	-0.1384	0.0710	0.0916	-0.0088	-0.1113
V1 $d_{z^2}$	0.0710	-0.0421	-0.1229	-0.0869	0.1506
V1 $d_{xy}$	0.0916	-0.1229	-0.2441	-0.1113	0.1198
V1 $d_{yz}$	-0.0088	-0.0869	-0.1113	-0.0348	-0.0383
V1 $d_{xz}$	-0.1113	0.1506	0.1198	-0.0383	0.0093

- [1] P. Fazekas, *Electron Correlation and Magnetism* (World Scientific, Singapore, 1999).
- [2] D. Khomskii, *Basic Aspects of the Quantum Theory of Solids* (Cambridge University Press, Cambridge, 2010).
- [3] R. Coldea, D. A. Tennant, K. Habicht, P. Smeibidl, C. Wolters, and Z. Tylczynski, Direct Measurement of the Spin Hamiltonian and Observation of Condensation of Magnons in the 2D Frustrated Quantum Magnet  $\text{Cs}_2\text{CuCl}_4$ , *Phys. Rev. Lett.* **88**, 137203 (2002).
- [4] G. Chaboussant, A. Sieber, S. Ochsenbein, H.-U. Güdel, M. Murrie, A. Honecker, N. Fukushima, and B. Normand, Exchange interactions and high-energy spin states in  $\text{Mn}_{12}$ -acetate, *Phys. Rev. B* **70**, 104422 (2004).
- [5] H. J. Silverstein, K. Fritsch, F. Flicker, A. M. Hallas, J. S. Gardner, Y. Qiu, G. Ehlers, A. T. Savici, Z. Yamani, K. A. Ross, B. D. Gaulin, M. J. P. Gingras, J. A. M. Paddison, K. Foyevtsova, R. Valenti, F. Hawthorne, C. R. Wiebe, and H. D. Zhou, Liquidlike correlations in single-crystalline  $\text{Y}_2\text{Mo}_2\text{O}_7$ : An unconventional spin glass, *Phys. Rev. B* **89**, 054433 (2014).
- [6] L. Savary, K. A. Ross, B. D. Gaulin, J. P. C. Ruff, and Leon Balents, Order by Quantum Disorder in  $\text{Er}_2\text{Ti}_2\text{O}_7$ , *Phys. Rev. Lett.* **109**, 167201 (2012).
- [7] H. Xiang, C. Lee, H.-J. Koo, X. Gong, and M.-H. Whangbo, Magnetic properties and energy-mapping analysis, *Dalton Trans.* **42**, 823 (2013).
- [8] O. Janson, J. Richter, and H. Rosner, Modified Kagome Physics in the Natural spin-1/2 Kagome Lattice Systems: Kapellasite  $\text{Cu}_3\text{Zn}(\text{OH})_6\text{Cl}_2$  and Haydeeite  $\text{Cu}_3\text{Mg}(\text{OH})_6\text{Cl}_2$ , *Phys. Rev. Lett.* **101**, 106403 (2008).
- [9] H. O. Jeschke, I. Opahle, H. Kandpal, R. Valentí, He. Das, T. Saha-Dasgupta, O. Janson, H. Rosner, A. Brühl, B. Wolf, M. Lang, J. Richter, S. Hu, X. Wang, R. Peters, T. Pruschke, and A. Honecker, Multistep Approach to Microscopic Models for Frustrated Quantum Magnets: The Case of the Natural Mineral Azurite, *Phys. Rev. Lett.* **106**, 217201 (2011).
- [10] K. Foyevtsova, I. Opahle, Y.-Z. Zhang, H. O. Jeschke, and R. Valentí, Determination of effective microscopic models for the frustrated antiferromagnets  $\text{Cs}_2\text{CuCl}_4$  and  $\text{Cs}_2\text{CuBr}_4$  by density functional methods, *Phys. Rev. B* **83**, 125126 (2011).
- [11] H. O. Jeschke, F. Salvat-Pujol, and R. Valentí, First-principles determination of Heisenberg Hamiltonian parameters for the spin-1/2 kagome antiferromagnet  $\text{ZnCu}_3(\text{OH})_6\text{Cl}_2$ , *Phys. Rev. B* **88**, 075106 (2013).
- [12] U. Tutsch, B. Wolf, S. Wessel, L. Postulka, Y. Tsui, H. O. Jeschke, I. Opahle, T. Saha-Dasgupta, R. Valentí, A. Brühl, K. Removic-Langer, T. Kretz, H.-W. Lerner, M. Wagner, and M. Lang, Evidence of a field-induced Berezinskii-Kosterlitz-Thouless scenario in a two-dimensional spin dimer system, *Nat. Commun.* **5**, 5169 (2014).
- [13] For a controversy about the magnitude of anisotropic spin-spin couplings in rare-earth pyrochlore systems, see Refs. [35,45–47].
- [14] A. Sadeghi, M. Alaei, F. Shahbazi, and M. J. P. Gingras, Spin Hamiltonian, order out of a Coulomb phase, and pseudocriticality in the frustrated pyrochlore Heisenberg antiferromagnet  $\text{FeF}_3$ , *Phys. Rev. B* **91**, 140407(R) (2015).
- [15] We are implicitly considering here the lowest-order nontrivial hopping processes and not discussing high-order ones giving rise, for example, to so-called ring (or cyclic) exchange.
- [16] L. Zhang, J. Ren, J.-S. Wang, and B. Li, Topological magnon insulator in insulating ferromagnet, *Phys. Rev. B* **87**, 144101 (2013).
- [17] A. Mook, J. Henk, and I. Mertig, Magnon Hall effect and topology in kagome lattices: A theoretical investigation, *Phys. Rev. B* **89**, 134409 (2014).
- [18] Y. Onose, T. Ideue, H. Katsura, Y. Shiomi, N. Nagaosa, and Y. Tokura, Observation of the Magnon Hall Effect, *Science* **329**, 297 (2010).
- [19] M. Elhajal, B. Canals, R. Sunyer, and C. Lacroix, Ordering in the pyrochlore antiferromagnet due to Dzyaloshinsky-Moriya interactions, *Phys. Rev. B* **71**, 094420 (2005).
- [20] T. Moriya, Anisotropic Superexchange Interaction and Weak Ferromagnetism, *Phys. Rev.* **120**, 91 (1960).
- [21] I. Dzyaloshinskii, A thermodynamic theory of “weak” ferromagnetism of antiferromagnetics, *J. Phys. Chem. Solids* **4**, 241 (1958).
- [22] M. Hirschberger, R. Chisnell, Y. S. Lee, and N. P. Ong, Thermal Hall Effect of Spin Excitations in a Kagome Magnet, *Phys. Rev. Lett.* **115**, 106603 (2015).
- [23] R. Chisnell, J. S. Helton, D. E. Freedman, D. K. Singh, R. I. Bewley, D. G. Nocera, and Y. S. Lee, Topological Magnon Bands in a Kagome Lattice Ferromagnet, *Phys. Rev. Lett.* **115**, 147201 (2015).
- [24] Ref. [18] estimated a spin stiffness  $D_s = -21 \text{ meV}\text{\AA}^2$ . The superexchange  $\mathcal{J} = -3.4 \text{ meV}$  can be obtained from the relationship  $\mathcal{J}S = 8D_s/a^2$  where  $S = 1/2$  is the spin value and  $a = 9.94 \text{\AA}$  is the size of the conventional cubic cell of  $\text{Lu}_2\text{V}_2\text{O}_7$ .
- [25] M. Mena, R. S. Perry, T. G. Perring, M. D. Le, S. Guerrero, M. Storni, D. T. Adroja, Ch. Rüegg, and D. F. McMorrow, Spin-Wave Spectrum of the Quantum Ferromagnet on the Pyrochlore Lattice  $\text{Lu}_2\text{V}_2\text{O}_7$ , *Phys. Rev. Lett.* **113**, 047202 (2014).
- [26] H. J. Xiang, E. J. Kan, M.-H. Whangbo, C. Lee, S.-H. Wei, and X. G. Gong, Single-ion anisotropy, Dzyaloshinskii-Moriya interaction, and negative magnetoresistance of the spin- $\frac{1}{2}$  pyrochlore  $\text{R}_2\text{V}_2\text{O}_7$ , *Phys. Rev. B* **83**, 174402 (2011).
- [27] Note that, although we chose for the sake of brevity, the labels  $\alpha$ ,  $\beta$  for the orbitals, it would be more correct to label them with an additional site index (e.g.,  $\alpha_i$ ,  $\beta_i$ ) since the orbitals are described in real space and therefore depend, due to the different local coordinate systems, on the specific site under consideration.
- [28] E. Pavarini, E. Koch, D. Vollhardt, and A. Lichtenstein, *The LDA+DMFT approach to strongly correlated materials*, Forschungszentrum Jülich GmbH; Institute for Advanced Simulations (2011).
- [29] K. Koepnick and H. Eschrig, Full-potential nonorthogonal local-orbital minimum-basis band-structure scheme, *Phys. Rev. B* **59**, 1743 (1999).
- [30] J. P. Perdew, K. Burke, and M. Ernzerhof, Generalized Gradient Approximation Made Simple, *Phys. Rev. Lett.* **77**, 3865 (1996).
- [31] M. Altmeyer, R. Valentí, and H. O. Jeschke, Role of layer packing for the electronic properties of the organic superconductor  $(\text{BEDT-TTF})_2\text{Ag}(\text{CF}_3)_4(\text{TCE})$ , *Phys. Rev. B* **91**, 245137 (2015).
- [32] D. Guterding, S. Backes, H. O. Jeschke, and R. Valentí, Origin of the superconducting state in the collapsed tetragonal phase of  $\text{KFe}_2\text{As}_2$ , *Phys. Rev. B* **91**, 140503(R) (2015).
- [33] H. Eschrig and K. Koepnick, Tight-binding models for the iron-based superconductors, *Phys. Rev. B* **80**, 104503 (2009).

- [34] A. A. Haghighirad, C. Gross, and W. Assmus, Powder synthesis and crystal growth of  $\text{Y}_2\text{V}_2\text{O}_7$  under high pressure and its physical properties, *Cryst. Growth* **310**, 2277 (2008).
- [35] K. A. Ross, L. Savary, B. D. Gaulin, and L. Balents, Quantum Excitations in Quantum Spin Ice, *Phys. Rev. X* **1**, 021002 (2011).
- [36] M. Blume and R. E. Watson, Theory of Spin-Orbit Coupling in Atoms. II. Comparison of Theory with Experiment, *Proc. Roy. Soc. (London) A* **271**, 565 (1963).
- [37] S. Shamoto, T. Nakano, Y. Nozue, and T. Kajitani, Substitution effects on ferromagnetic Mott insulator  $\text{Lu}_2\text{V}_2\text{O}_7$ , *J. Phys. Chem. Solids* **63**, 1047 (2002).
- [38] D. Khomskii, *Transition metal compounds* (Cambridge University Press, Cambridge, 2014).
- [39] S. Miyahara, A. Murakami, and N. Furukawa, Orbital ordering induced ferromagnetism in  $\text{Lu}_2\text{V}_2\text{O}_7$ , *J. Mol. Struct.* **838**, 223 (2007).
- [40] D. Szczepanik and J. Mrozek, On several alternatives for Löwdin orthogonalization, *Comput. Theor. Chem.* **1008**, 15 (2013).
- [41] I. Lindgren and J. Morrison, *Atomic many-body theory* (Springer, Berlin, 1986).
- [42] S. M. Winter, Y. Li, H. O. Jeschke, and R. Valentí, Challenges in design of Kitaev materials: Magnetic interactions from competing energy scales, *Phys. Rev. B* **93**, 214431 (2016).
- [43] J. G. Rau, L. S. Wu, A. F. May, L. Poudel, B. Winn, V. O. Garlea, A. Huq, P. Whitfield, A. E. Taylor, M. D. Lumsden, M. J. P. Gingras, and A. D. Christianson, Anisotropic Exchange within Decoupled Tetrahedra in the Quantum Breathing Pyrochlore  $\text{Ba}_3\text{Yb}_2\text{Zn}_5\text{O}_{11}$ , *Phys. Rev. Lett.* **116**, 257204 (2016).
- [44] A. I. Liechtenstein, V. I. Anisimov, and J. Zaanen, Density functional theory and strong interactions: Orbital ordering in Mott-Hubbard insulators, *Phys. Rev. B* **52**, R5467(R) (1995).
- [45] J. D. Thompson, P. A. McClarty, H. M. Rønnow, L. P. Regnault, A. Sorge, and M. J. P. Gingras, Rods of Neutron Scattering Intensity in  $\text{Yb}_2\text{Ti}_2\text{O}_7$ : Compelling Evidence for Significant Anisotropic Exchange in a Magnetic Pyrochlore Oxide, *Phys. Rev. Lett* **106**, 187202 (2011).
- [46] J. Robert, E. Lhotel, G. Remenyi, S. Sahling, I. Mirebeau, C. Decorse, B. Canals, and S. Petit, Spin dynamics in the presence of competing ferromagnetic and antiferromagnetic correlations in  $\text{Yb}_2\text{Ti}_2\text{O}_7$ , *Phys. Rev. B* **92**, 064425 (2015).
- [47] L. D. C. Jaubert, O. Benton, J. G. Rau, J. Oitmaa, R. R. P. Singh, N. Shannon, and M. J. P. Gingras, Are Multiphase Competition and Order by Disorder the Keys to Understanding  $\text{Yb}_2\text{Ti}_2\text{O}_7$ ?, *Phys. Rev. Lett.* **115**, 267208 (2015).